Academic Journal of Science and Technology
ISSN: 2771-3032 | Vol. 8, No. 2, 2023

Study on the Influence of Structure and Material Parameters on Dynamic Sealing Characteristics of Composite Seal Ring

Chao He*, Zhilin Li

Drilling & Production Engineering Technology Research Institute, CNPC Chuanqing Drilling Engineering Co., Ltd., Guanghan, 6183001, China

* Corresponding author

Abstract: Aiming at the failure problem of composite sealing ring, the influence of elastic modulus of carbon fiber content, groove width and number of grooves on dynamic sealing characteristics of sealing ring was analyzed by finite element method. The results showed that the maximum stress after precompression was located in the middle of the contact between slip ring and O ring, and the maximum contact pressure was located to the left of the inner circle of slip ring. After applying the fluid pressure, the maximum stress is located at the right side of the contact between the slip ring and O ring and the middle part of the contact between the slip ring and O ring, and the maximum contact pressure is located at the middle part of the inner circle of the slip ring. In dynamic sealing state, the magnitude and position of the maximum contact pressure and the maximum stress of left and right stroke are basically the same; The width and number of grooves increase the contact pressure and stress, but the width of groove interval is opposite.

Keywords: Von-Mises stress; Contact pressure; Combination sealing ring; Sealing characteristics; The finite element.

1. Introduction

Hydraulic transmission systems exhibit notable advantages such as high power output, smooth transmission, and superior acceleration characteristics. In this context, sealing technology stands as a crucial component within hydraulic transmissions, as the quality of sealing directly determines the operational reliability of hydraulic products. A substantial body of engineering cases underscores that hydraulic systems encounter failure rates as high as 50% due to seal component malfunction. The losses incurred as a consequence of seal component failure far surpass the intrinsic value of the seal itself. Composite seals effectively amalgamate the excellent wear resistance properties of PTFE materials with the self-sealing attributes of rubber materials, representing a prevailing trend in the development of reciprocating seals. Consequently, the investigation of key parameters influencing the sealing performance of composite seal structures assumes paramount significance.

Cui et al. [1], using Abaqus, investigated the static sealing characteristics of a two-dimensional axisymmetric model of Y-shaped seal rings. Their findings indicated that with increasing pressure, stress levels increased, and the maximum contact pressure was concentrated at the contact points between the reciprocating rod and the seal groove bottom. GU et al.[2] employed finite element analysis to assess the static sealing performance of rubber seal rings. Their results showed that when the compression amount reached 2.5mm, the maximum contact pressure of the rubber seal ring was concentrated on both sides of the seal ring. Bhaumik et al.[3] utilized finite element methods to study the static sealing characteristics of U-shaped seal rings. They found that frictional forces decreased with increasing velocity, and there was a high degree of correlation between experimental and finite element analysis results regarding frictional forces. Bhaumik et al.[4] utilized finite element methods to study the static sealing characteristics of U-shaped seal rings. They found that frictional forces decreased with increasing velocity, and there was a high degree of correlation between experimental and finite element analysis results regarding frictional forces. Mazza et al.[5] analyzed the frictional behavior of two-dimensional axisymmetric models of reciprocating seal rings, proposing solutions to address the combined effects of friction coefficients and motion direction on frictional forces. Azza et al.[6] analyzed the frictional behavior of two-dimensional axisymmetric models of reciprocating seal rings, proposing solutions to address the combined effects of friction coefficients and motion direction on frictional forces. Yokoyama et al.[7] studied the static sealing characteristics of two-dimensional axisymmetric models of O-shaped seal rings through numerical simulation methods. They found that contact pressure increased with an increase in medium pressure. Han Ning conducted rotational motion analysis of O-shaped seal rings in a three-dimensional model using Abaqus, studying the impact of hydraulic pressure and rotational speed on the Von Mises stress and contact pressure[8]. Li Dan performed an analysis of the static and dynamic sealing performance of leaft-type seal rings in a two-dimensional axisymmetric model using Ansys. They studied the influence of compression ratio, friction coefficient, groove clearance, and working pressure on Von Mises stress and contact pressure[9]. Bai Guicai and Shentu Liufang conducted a study using Abaqus on the static sealing performance of double-layer ring-type composite seal rings in a two-dimensional axisymmetric model. They investigated the influence of medium pressure and compression ratio on Von Mises stress and contact pressure[10]. Zhang Fuying, Sun Yujia, and Jiang Xiangmin used Ansys to study the static sealing and reciprocating dynamic sealing performance of square coaxial composite seal rings in a two-dimensional axisymmetric model. They determined the influence of compression ratio, sealing ring thickness, sealing ring bottom

chamfer, sealing ring top chamfer on the maximum Von Mises stress and maximum contact pressure in static sealing state. They also examined the influence of piston rod operating speed, sealing ring friction coefficient on the maximum Von Mises stress and maximum contact pressure in dynamic sealing state[11]. Li Jiwei et al.[12] conducted a study on the reciprocating sealing performance of rubber O-shaped seal rings in a two-dimensional axisymmetric model using finite element software. They investigated the influence of material properties, the presence of transition arcs, friction coefficients, and assembly speed on shear stress. Zhang Liying et al.[13] used Ansys to investigate the reciprocating sealing performance of polyurethane leaft-type seal rings in a two-dimensional axisymmetric model. They studied the impact of medium pressure on the maximum Von Mises stress and maximum contact pressure during the piston rod's outward and inward strokes. Liu Qingyou, Yang Yaqiang, Zhu Haiyan, and others[14] studied the static sealing performance and reciprocating dynamic sealing performance of C-shaped ring composite seal rings in a two-dimensional axisymmetric model using Abaqus. They examined the influence of sealing clearance and working pressure on Von Mises stress and contact pressure in the static sealing state and investigated the impact of working pressure, friction factor, reciprocating speed, and sealing clearance on Von Mises stress and contact pressure in the dynamic sealing state. Zeng Youkui analyzed the Von Mises stress, shear stress, and contact pressure of composite seal rings in a three-dimensional model under installation, static sealing, and rotational sealing states using Ansys. The study revealed the effects of arc radius, O-ring diameter, friction coefficient on sealing surface, compression amount, and eccentricity of the shaft and end cap on Von Mises stress, shear stress, and contact pressure of composite seal rings[15]. Shi Leilei et al.[16] utilized Ansys to investigate the static sealing performance of rubber plum blossom-shaped seal rings in a three-dimensional model. They determined the influence of friction factors, medium pressure, and compression ratio on contact pressure and Von Mises stress. Yi Pan, Jin Yongping, and others[17] conducted an Abaqus-based study on the static sealing performance of full-fluororubber slip ring composite seal rings in a two-dimensional axisymmetric model. They established the impact of hydraulic pressure on Von Mises stress and contact pressure. Guo Jianzhang et al.[18] studied the patterns of contact pressure and Von Mises stress of smooth and non-smooth seal rings concerning pit diameter and spacing. They found that the presence of biomimetic pits did not adversely affect seling characteristics, and a favorable pit distribution promoted friction and wear characteristics.

The above-mentioned research findings highlight extensive investigations into the sealing characteristics of various seal ring configurations using advanced numerical and analytical methods. These studies provide valuable insights into the factors affecting sealing performance under static and dynamic conditions, offering essential guidance for future research and practical applications in the field of fluid dynamics and mechanical engineering.

2. Numerical Simulation Model Establishment

The Yeoh model performs well in characterizing small deformations of rubber materials and is commonly chosen as the preferred numerical simulation model within the small deformation range in engineering. Accordingly, this study has selected rubber material parameters with C1=2.46, C2=0.085, and D=-0.0021. The composite seal ring is composed of a groove, shaft, sliding ring, and O-ring, with dimensional parameters referencing the Chevron seal TB4-IB120X5.7. The friction coefficient is 0.04, and the other material and mechanical parameters are as shown in Table 1.

Table 1. Composite Seal Ring Material and Mechanical Parameters

Material type		axle 42CrMo	groove 42CrMo	collector ring polytetrafluoroethylene
mechanical parameter	Young's modulus	212GPa	212GPa	960MPa
	Poisson's ratio	0.28	0.28	0.45
	densities	7850kg/m³	7850kg/m³	2320kg/m³

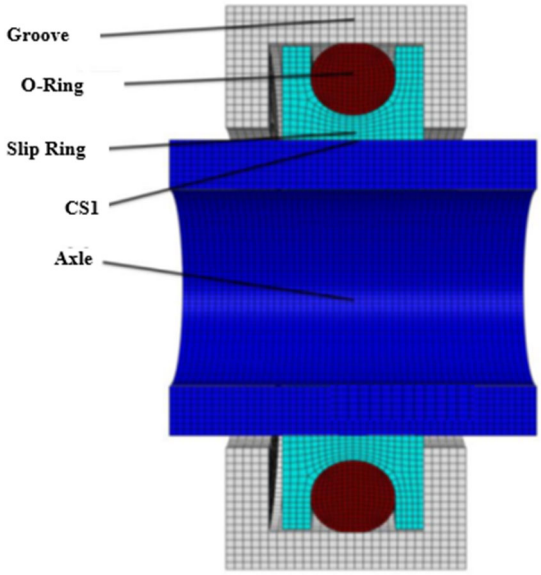

Figure 1. Numerical simulation model

The model was divided into a hexahedral mesh, and the post-division results are shown in Fig.1. The axial motion process is divided into left and right strokes, with the left stroke having a velocity direction opposite to the fluid pressure direction, and vice versa for the right stroke. The analysis of the sealing performance of the composite seal ring is conducted using the following steps:

(1) A radial displacement of 0.45mm is applied to the groove to achieve precompression;

(2) A fluid pressure of 5MPa is applied to the working surface of the composite seal ring to achieve static sealing. Dynamic sealing is achieved by simultaneously applying a reciprocating velocity V=0.3m/s and a rotational velocity n=150r/min on top of the static sealing conditions. CS1 sealing surface (the primary sealing surface) is the focus of this study.

3. Results and Discussion

Fig.2 and Fig.3 depict stress distributions for static sealing and dynamic sealing of the sealing ring, respectively. As inferred from the diagrams, post-preloading, the maximum stress is situated in the central region of contact between the sealing ring and the O-ring, whereas the maximum contact pressure is located to the left of the inner circle of the sealing ring. Upon the application of fluid pressure, the maximum stress shifts to the right side of the contact area between the sealing ring and the O-ring, as well as the central region of their contact. Simultaneously, the maximum contact pressure transitions towards the central region of the inner circle of the sealing ring. Notably, the maximum contact pressure of 14.91 MPa significantly exceeds the fluid pressure, thereby enabling effective sealing. In the dynamic sealing state, the magnitudes and positions of the maximum contact pressure and maximum stress during both left and right strokes are essentially identical

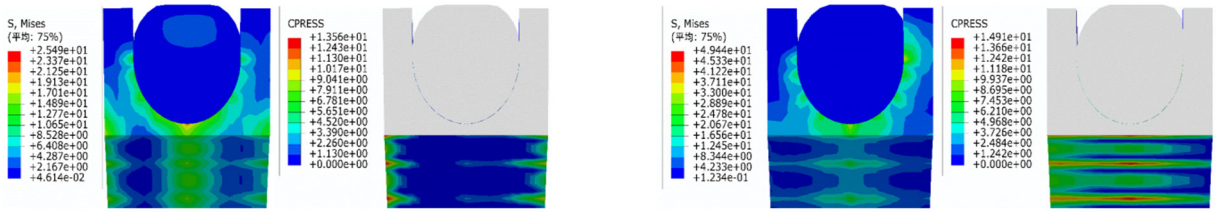

(a) pre-compression (b) fluid pressure

Figure 2. Static seal stress diagram

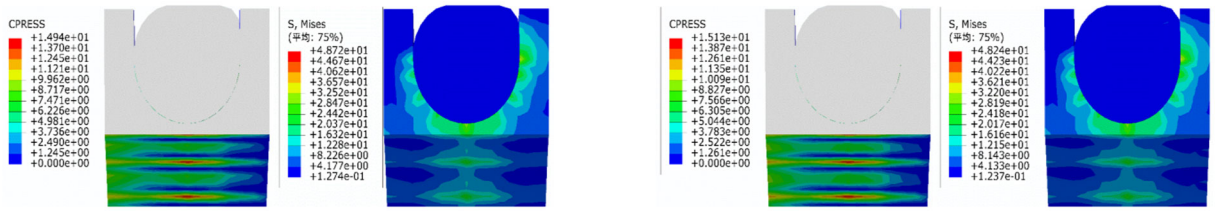

(a) left-hand side (b) right-hand side

Figure 3. Dynamic seal stress diagram

Fig.4 illustrates stress distributions corresponding to different values of elastic modulus. From the diagram, it can be observed that stress levels and contact pressures during both left and right strokes increase with an increase in the elastic modulus. The stress during the left stroke consistently exceeds that during the right stroke, and stress exhibits a nearly linear growth pattern with an increase in elastic modulus. Additionally, the difference in stress values gradually enlarges. In contrast, the relationship between contact pressure and elastic modulus is nonlinear, with the growth rate initially decreasing, followed by an increase, and then a subsequent decrease. Moreover, for elastic modulus values less than 910 MPa, the contact pressure during the right stroke is generally higher than that during the left stroke, although the contact pressure still exceeds the fluid pressure of 5 MPa.

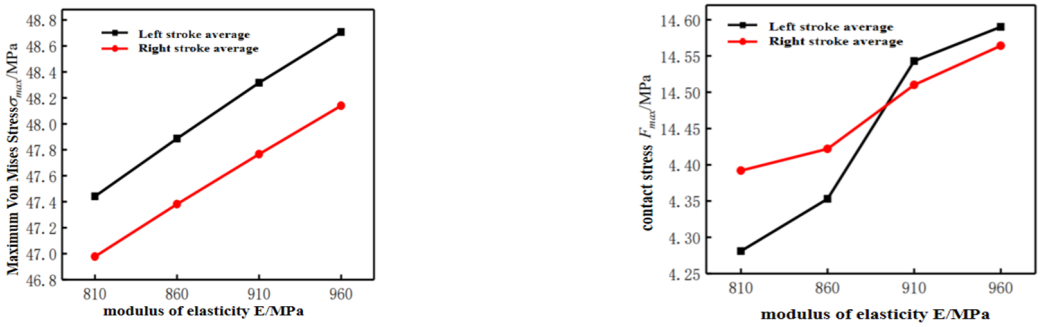

(a) Von Mises stresses (b) contact pressure

Figure 4. Stress diagram for different elastic moduli

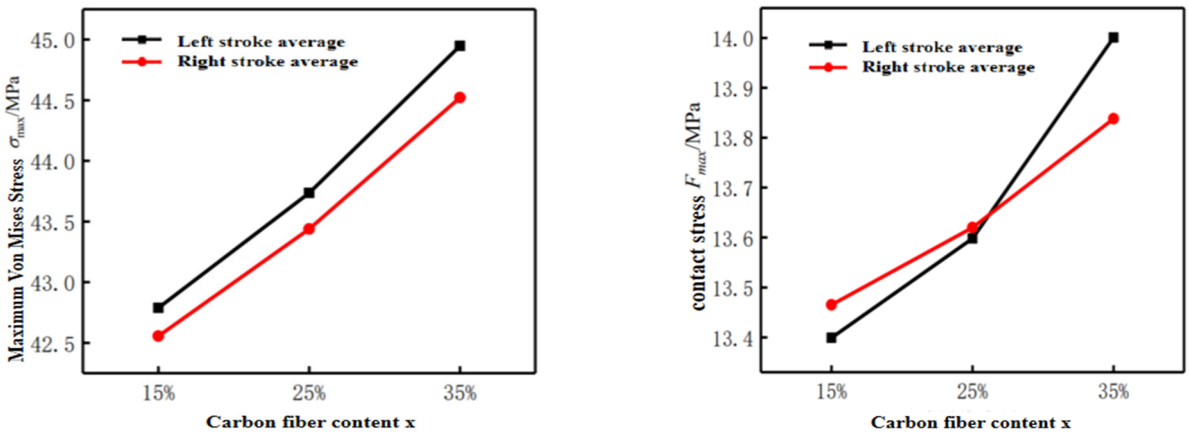

(a) Von Mises stresses (b) contact pressure

Figure 5. Stress diagram of different carbon fiber content

Fig.5 presents stress distributions for various carbon fiber content levels. From the diagram, it is evident that an increase in carbon fiber content results in higher stress levels, greater stress differences, and increased stress growth rates. Moreover, stress during the left stroke surpasses that during the right stroke. Contact pressure and its growth rate also exhibit an increasing trend with the augmentation of carbon fiber content. Furthermore, the difference in contact pressure initially decreases and then increases as carbon fiber content rises. For carbon fiber content levels below 25%, the contact pressure during the right stroke is higher than that during the left stroke, whereas for levels exceeding 25%, the contact pressure during the left stroke exceeds that during the right stroke.

Fig.6 displays stress distributions for different values of Poisson's ratio. From the graph, it is evident that stress varies inversely with Poisson's ratio and generally follows a linear pattern. The difference in stress values increases as Poisson's ratio increases, with stress during the left stroke consistently exceeding that during the right stroke. Contact pressure primarily demonstrates an increasing trend as Poisson's ratio increases. However, the difference in contact pressure and its growth rate exhibit a decreasing pattern. For Poisson's ratios below 0.41, the contact pressure during the right stroke is higher than that during the left stroke, while for Poisson's ratios greater than 0.41, the contact pressure during the left stroke exceeds that during the right stroke.

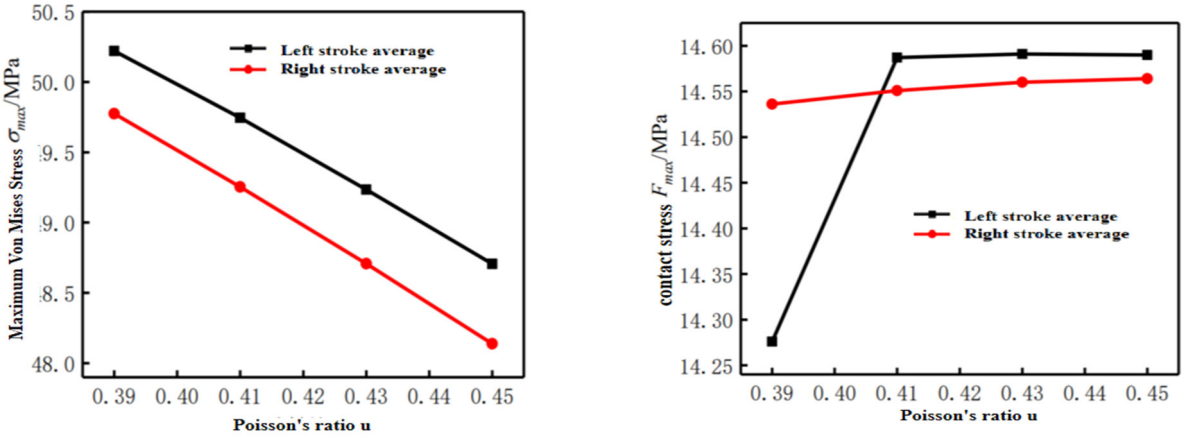

(a) Von Mises stresses (b) contact pressure

Figure 6. Different Poisson's Ratio Stress Plot

Based on reference [19], it is established that internal grooving within the sealing ring not only facilitates the storage of impurities but also enhances sealing performance by reducing the contact area. Subsequently, this study investigates the impact of various parameters related to triangular grooves inside the sealing ring on its sealing performance. Fig.7 illustrates stress distributions for different numbers of grooves in static sealing.From the diagram, it can be observed that after the application of pressure, the maximum stress is located in the central and right-side regions of the contact between the sealing ring and the O-ring. The maximum contact pressure occurs in the central region of contact between the sealing ring and the shaft, with the maximum contact pressure surpassing the fluid pressure, ensuring reliable sealing. Both contact pressure and stress increase as the number of grooves rises, primarily due to the significant deformation induced by a higher groove count.

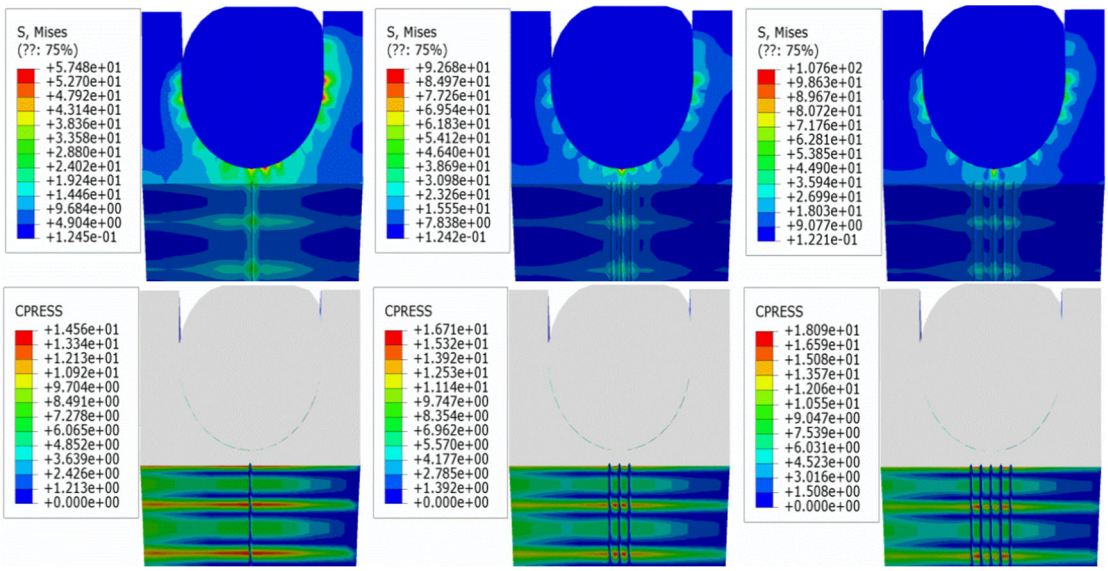

(a) Z=1 (b) Z=3 (c) Z=5

Figure 7. Static sealing stress diagram for different numbers of grooves

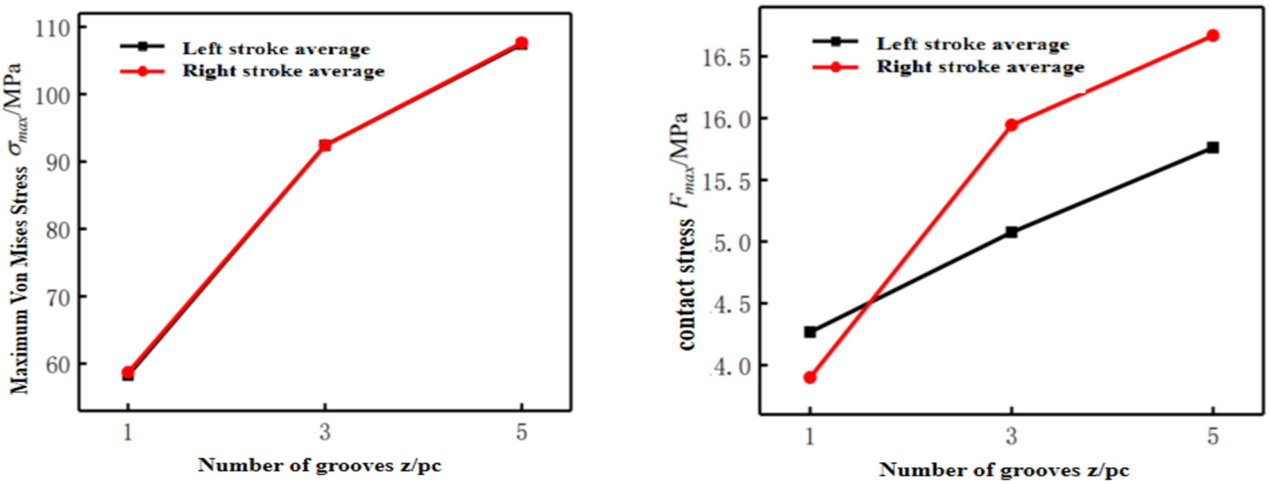

(a) Von Mises stresses (b) contact pressure

Figure 8. Stress diagram for different number of grooves

Fig.8 presents stress distributions for different numbers of grooves. From the graph, it is evident that stress exhibits a proportional increase with an increase in the number of grooves, while the stress difference remains relatively constant. However, the rate of stress growth gradually decreases, with the stress levels during the left and right strokes being nearly equal. As the number of grooves increases, contact pressure and its difference become larger. The growth rate of contact pressure during the left stroke remains relatively constant, but during the right stroke, it initially increases and then decreases. When the number of grooves is less than 3, the contact pressure during the left stroke exceeds that during the right stroke, whereas when the number of grooves exceeds 3, the contact pressure during the right stroke becomes higher than that during the left stroke.

Fig.9 illustrates stress distributions for different groove widths. From the graph, it can be observed that stress generally follows a nonlinear increase as groove width expands, with the stress growth rate gradually increasing. The stress difference remains relatively constant, and stress levels during the left and right strokes are approximately equal. Contact pressure shows a proportional increase with groove width. The difference in contact pressure exhibits a pattern of decreasing, then increasing, and finally decreasing again. Additionally, the growth rate of contact pressure during the left stroke is generally greater than that during the right stroke. Throughout, the contact pressure during the right stroke consistently exceeds that during the left stroke.

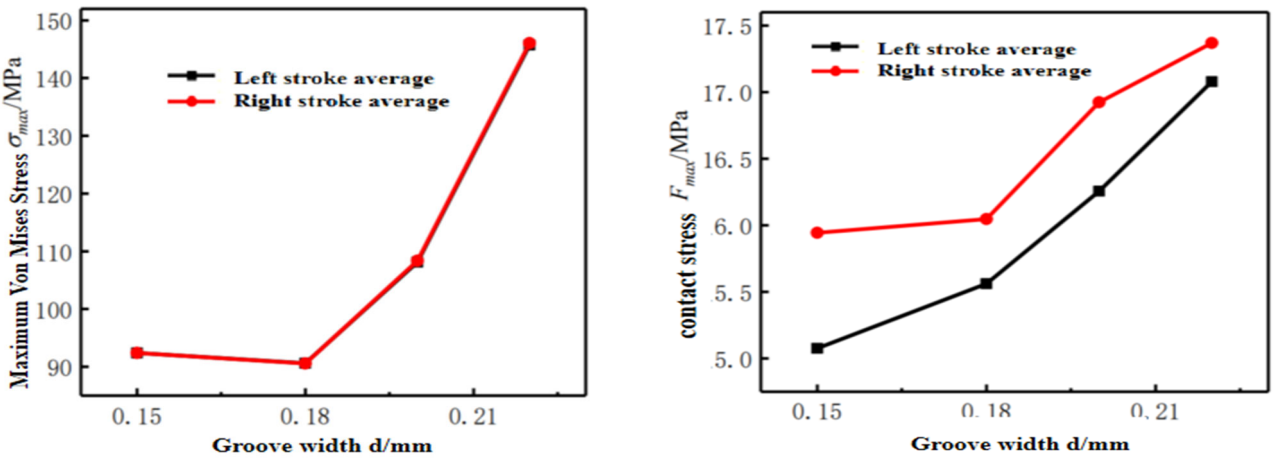

(a) Von Mises stresses (b) contact pressure

Figure 9. Stress diagram for different groove widths

Fig.10 presents stress distributions for different groove spacing widths. From the graph, it is evident that as the groove spacing width increases, stress gradually decreases, while the stress difference remains relatively constant. The rate of stress change gradually increases, and stress levels during the left and right strokes are approximately equal. Contact pressure exhibits an inverse proportional relationship with groove spacing width. The difference in contact pressure and its rate of change gradually decrease. For groove spacing widths less than 0.6 mm, the contact pressure during the right stroke is higher than that during the left stroke, whereas for groove spacing widths greater than 0.6 mm, the situation reverses.

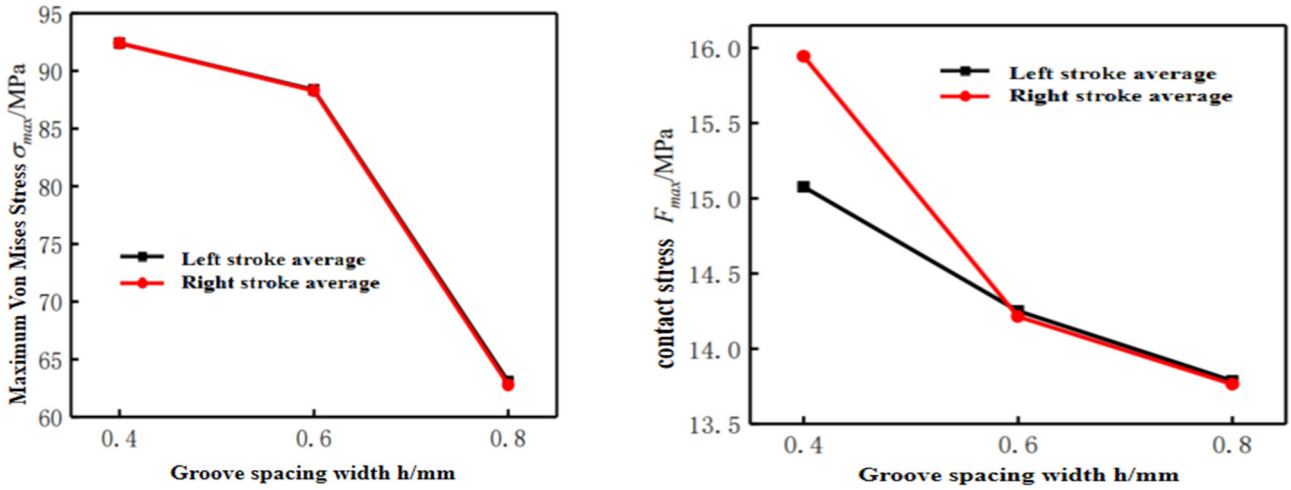

(a) Von Mises stresses (b) contact pressure

Figure 10. Stress diagram for different trench spacing widths

4. 4.Conclusions

(1) After pre-compression, the maximum stress is located in the middle section of the contact between the sealing ring and the O-ring, and the maximum contact pressure is located on the left side of the inner circle of the sealing ring. Upon the application of fluid pressure, the maximum stress is located on the right side of the contact between the sealing ring and the O-ring and in the middle section of this contact, with the maximum contact pressure located in the middle section of the inner circle of the sealing ring. In the dynamic sealing state, the magnitudes and locations of the maximum contact pressure and maximum stress on the left and right strokes are essentially the same.

(2) Stress and contact pressure increase with an increase in elastic modulus, carbon fiber content, groove width, and the number of grooves, while they decrease with an increase in groove spacing width. Additionally, stress decreases with an increase in Poisson's ratio, while contact pressure exhibits the opposite trend.

References

[1] Cui,KB.,Qin,JQ.,Di,CC., et al. Finite E–lement Analysis and Simulation of the Sealing Performance of Y-Ring Rubber Seal[J]. AppliedMechanics & Materials, 2013,444-445:1379-1383.

[2] Gu,YQ.,Zhao,G.,Liu,H., et al. Characteristics of seal shell body's rubber ring with bionic dimpled surfaces of aerodynamic extinguishing cannon[J]. Journal of Central South U–niversity, 2013, 20(11):3065-3076.

[3] Bhaumik,S., Kumar,SR., Kumaraswamy A., Exp–erimental Investigation and FE Modelling of Contact Mechanics Phenomenon in Reciprocating Hydraulic U-Seals for Defence Applications[J]. Applied Mechanics & Materials, 2014, 592-594: 1950-1954.

[4] [4] Nikas, GK., Elastohydrodynamics and Mechanics of Rectangular Elastomeric Seals for Reciprocating Piston Rods[J]. journal of tribology, 2003, 125(1):60-69.

[5] Mazza, LG., Belforte,et al. Analytical/Experimental Study of the Contribution of In–dividual Seals to Friction Force in Pneumatic Actuators[J]. Journal of Tribology, 2017.

[6] Azzi,A., Maoui, A., Fatu, A., et al. Exper–imental study of friction in pneumatic seals[J]. Tribology International, 2019.

[7] Yokoyama,K., Okazaki,M., Komito,T., Effect of contact pressure and thermal degradation on the sealability of O-ring[J]. Jsae Review, 1998, 19(2):123-128.

[8] Han,N., Sealing performance analysis of dynamic sealing system[D]. North Central University,2014.

[9] Li,D., Research on numerical analysis method of sealing performance of hydraulic cylinder[D]. Xi'an University of Science and Technology,2015.

[10] Bai,GC.,Shen,T., Liu,F., The finite element analysis of transmission double ring type combined seal structure[J]. Modern Manufacturing Engineering,2015(01):74-77.

[11] Zhang,FY.,Sun,YJ.,Jiang XM., Optim–ization of the structure and operating param–eters of rectangular coaxially combined seal[J]. Journal of Tianjin University of Science & Technology, 2016,31(04):60-64.

[12] Li,JW.,Cao JW.,Wang GR.,et al. Param–eter analysis of assembling rubber O ring ba–sed on finite element[J]. Aero Weaponry,2017(06):72-76.

[13] Zhang,LY.,Zhang,PP.,Zhang,ZY., Analysis on finite element numerical simulation of budshaped seal ring based on ANSYS software[J]. Shanxi Coking Coal Science & Technology, 2017,41(12):15-18.

[14] Liu,QY.,Yang,YQ.,Zhu,HY.,et al. Sealing performance of C-sliding ring combined seals [J]. Lubrication Engineering, 2017, 42(08):36-41.

[15] Zeng,YK., Research on the performance of U-shaped combination seal for marine equipment[D]. Xi'an University of Science and Technology,2017.

[16] Shi,LL., Lu,LQ., Tang,YL., et al. Finite element analysis of sealing performance of plum blossom-shaped seals[J]. Journal of Guangxi University (Natural Science Edition), 2018, 43(02): 480-487.

[17] Yi,P.,Jin Yp.,Peng YD., et al. Perf–ormance analysis of combined seal structure in deep sea high pressure environment[J]. Jour–nal of Hunan University of Science & Technol–ogy(Natural Science Edition),2018,33(02):34-39.

[18] Guo,JZ.,Wang,YC., Finite element analysis of non-smooth seals with bionic pits[J]. Industrial Safety and Environmental Protection,2020,46(02):79-82.

[19] Ma,J.,Zhao,HQ.,Zhang,YC.. Design and finite element analysis of the combined seal structure of a high pressure screw conveyor[J]. Journal of Beijing University of Chemical Technology(Natural Science Edition), 2013(2):85-89.